Influence of nitrogen stoichiometry and the role of Sm 5*d* states in SmN thin films

A. Meléndez-Sans,[1] V. M. Pereira,[1] C. F. Chang,[1] C.-Y. Kuo,[1,2,3] C. T. Chen,[2] L. H. Tjeng,[1] and S. G. Altendorf[1]

[1]*Max Planck Institute for Chemical Physics of Solids, Nöthnitzer Straße 40, 01187 Dresden, Germany*

[2]*National Synchrotron Radiation Research Center, 101 Hsin-Ann Road, 30076 Hsinchu, Taiwan*

[3]*Department of Electrophysics, National Yang Ming Chiao Tung University, 30010 Hsinchu, Taiwan*

(Received 26 April 2024; revised 17 June 2024; accepted 20 June 2024; published 11 July 2024)

We report a comprehensive study of the synthesis of epitaxial SmN thin films on $LaAlO_3$ (100) by molecular beam epitaxy under slow-growth conditions. By carefully tuning the substrate temperature and the molecular nitrogen partial pressure, we are able to control the nitrogen content of our samples and produce near-stoichiometric, well-ordered SmN thin films. The influence of nitrogen defects on the samarium ion valence and the electronic structure is investigated by x-ray absorption and photoelectron spectroscopy, suggesting that the empty Sm 5*d* states may act as a charge reservoir stabilizing the $4f^5$ configuration in the nitrogen-deficient compound. The spectra also reveal a significant hybridization of the Sm $4f$ and N $2p$ states.

DOI: 10.1103/PhysRevB.110.045120

I. INTRODUCTION

Rare earth mononitrides combine interesting magnetic and semiconducting properties. The strong exchange interaction in the magnetic low-temperature phase can cause significant opposite spin splitting in both the rare earth 5*d* conduction and nitrogen 2*p* valence band edges. Charge carriers due to electron or hole doping are therefore expected to be largely spin polarized [1]. This makes them attractive candidates for spintronic devices as a proof of concept or even for potential applications [2–6], renewing interest in this class of materials, especially in thin film form.

Samarium nitride (SmN) stands out in the rare earth nitride series because of its near-zero magnetic moment. While early experimental bulk susceptibility and magnetization measurements described SmN as antiferromagnetic with a Néel temperature of ≈13–15 K [7,8], more recent thin film magnetization and x-ray magnetic circular dichroism studies described it as a ferromagnetic semiconductor with a Curie temperature of ≈27–38 K and a near-zero moment of $0.035\mu_B$ per Sm ion due to a near cancellation of spin and orbital contributions [9–11]. Such zero net moment materials can be advantageous for device applications, such as magnetic memory elements, due to the absence of stray fields, robustness to demagnetization forces, and expected small critical currents required for spin-transfer torque switching [12].

Like other rare earth nitrides, SmN crystallizes in the fcc rocksalt structure. It has a bulk lattice constant of 5.0481 Å [13]. The semiconducting nature of SmN thin films was confirmed by resistivity measurements [14] and optical spectroscopy, which indicates a band gap of 1.27 eV [15]. Small deviations in the nitrogen stoichiometry can cause drastic changes in the electrical transport properties. SmN thin films have even been observed to become superconducting below 4 K for carrier concentrations above 10^{21} cm^{-3}, which has been associated with nitrogen vacancy concentrations on the order of a few percent [16].

Unlike most rare earths, which generally have a stable 3+ valence, samarium can also adopt the 2+ valence state. Here we note that in the rare earth research community, the rare earth valence commonly refers to the $4f$ state, in which Sm^{3+} has the $[Xe]4f^55d^0$ configuration and Sm^{2+} has the $[Xe]4f^65d^0$ configuration. On the one hand, this degree of freedom in the valence can complicate sample preparation and understanding of the properties; on the other hand, it is interesting to investigate the $4f$ configuration of Sm in the SmN lattice, particularly what happens when nitrogen vacancies are present and how their presence affects the electronic structure overall.

Despite the tremendous progress in thin film technology in recent decades, research on SmN and on rare earth nitrides in general is still challenging, as reflected by many conflicting results and unresolved questions. The controversies are generally attributed to the poorly controlled stoichiometry and the highly air sensitive nature of these materials [1]. The preparation of epitaxial thin films [11,17–25] is further complicated by the limited availability of substrates with the same crystal structure and lattice parameters that do not react with the rare earths. This often results in significant roughness due to defects caused by lattice mismatch with the substrate or due to the formation of parasitic interfacial layers.

Surprisingly, although control of the composition has been recognized as critical, only a few detailed reports on the growth of rare earth nitride films exist [11,17,18,22,24]. While these studies provide relevant initial insights into the growth of rare earth nitrides, it is important to note that many of them still suffer from sample quality issues. In addition to the lack

of suitable substrates mentioned above, the high evaporation and growth temperatures and nitrogen pressures usually reported, as well as the fast deposition rates and the use of nitrogen precursors or activated nitrogen gas, may be additional sources of defects. Moreover, a thorough description of the growth process is generally not provided.

In this work, we systematically investigate the growth of SmN by molecular beam epitaxy (MBE) at ultrahigh-vacuum base pressures, using moderate molecular nitrogen pressures and deposition temperatures and slow growth rates. The relatively low evaporation temperature of samarium allows the use of a standard effusion cell, which only slightly increases the base pressure. Using these clean conditions, we aim for maximum control of the composition with low defect concentration, which is important to study and understand the intrinsic nature of the material [26].

As a substrate, we use $LaAlO_3$ (100), which has a pseudocubic lattice constant of about 3.8 Å; i.e., the lattice mismatch of SmN with the substrate is significant, about 6% when considering a 45° rotation, but much smaller than, e.g., that for MgO (100) [17]. In addition, $LaAlO_3$ is known to be chemically stable, preventing interfacial reactions observed for the growth on yttria-stabilized zirconia (YSZ) (001) [23], GaN (0001) [27], and Si (100) [11]. Thus, the choice of $LaAlO_3$ (100) is expected to allow an improved degree of purity and crystallinity for the deposited SmN films. In fact, the epitaxial growth of rare earth nitrides on $LaAlO_3$ (100) substrates was recently demonstrated [26,28].

The influence of the growth conditions on the composition (nitrogen content) and the samarium valence, more precisely the $4f$ configuration, as well as on the crystalline and electronic structure was monitored by *in situ* reflection high-energy electron diffraction, x-ray and ultraviolet photoelectron and x-ray absorption spectroscopy, and *ex situ* x-ray diffraction.

II. EXPERIMENT

SmN thin films were grown by MBE on epi-polished $LaAlO_3$ (LAO) (100) substrates purchased from Crystal GmbH. Prior to deposition, the substrates were annealed *in situ* in a separate chamber for 2 h at 500–600 °C in an oxygen atmosphere of 1×10^{-6} mbar to achieve a clean and well-ordered substrate surface.

One of the MBE systems at the Max Planck Institute for Chemical Physics of Solids is equipped with six effusion cells and a leak valve. High-purity Sm metal, additionally refined at 1000 °C in a Mo or Ta ampoule before use, was evaporated from a standard effusion cell. The Sm flux rate was measured at the growth position prior to deposition using a quartz crystal monitor and was set to approximately 1 Å/min ($T_{Sm} \approx 535$ °C). We note that the Sm sublimation rate at constant temperature of the effusion cell may decrease slightly when high nitrogen pressures are supplied during growth. Thorough degassing of the samarium material ensured that the background pressure rose only slightly to about 2×10^{-10} mbar at the evaporation temperature. During deposition, high-purity molecular nitrogen (6.0) was supplied via a leak valve. Samarium, like most rare earth elements, has a catalytic dissociative effect that allows it to react with molecular nitrogen to form SmN layers on the growing surface [29]. Different substrate temperatures T_{sub} and nitrogen partial pressures P_{N_2} were chosen for each film. Unless otherwise stated, the growth time was set to 2 h.

The samples were characterized *in situ* by reflection high-energy electron diffraction (RHEED), x-ray photoelectron spectroscopy (XPS), and ultraviolet photoelectron spectroscopy (UPS). A STAIB Instruments RH35 system with the kinetic energy set at 20 keV was used for the RHEED measurements. Monochromatic Al $K\alpha$ light (photon energy = 1486.6 eV) was used for the XPS measurements, and a nonmonochromatic He discharge lamp (photon energy = 21.2 eV, He I line) was used for the UPS measurements. A Scienta R3000 electron energy analyzer was used for XPS and UPS. The data were acquired at room temperature in normal emission geometry, with energy resolutions of about 0.35 eV for XPS and about 0.1 eV for UPS. The growth and *in situ* characterization were performed under UHV conditions, with a base pressure of about 1×10^{-10} mbar.

Ex situ x-ray diffraction (XRD) measurements were performed to further characterize the crystalline structure of the films. To prevent degradation in air, the films were capped *in situ* with a 10 nm layer of Cr prior to removal from the UHV system. The XRD data were collected using a PANalytical X'Pert PRO diffractometer with monochromatic Cu $K\alpha_1$ radiation ($\lambda = 1.540\,56$ Å).

Additional *in situ* x-ray absorption (XAS) and XPS measurements were performed at the TPS 45A beamline of the National Synchrotron Radiation Research Center (NSRRC) in Taiwan. The samples were measured at room temperature in total electron yield mode for XAS and in normal emission geometry with a photon energy of 1400 eV and an energy resolution of about 0.2 eV for XPS. As energy references for the Sm $M_{4,5}$ and the N K absorption edges, the Eu M_5 edge of $EuCoO_3$ and the Ti $L_{2,3}$ edges of $SrTiO_3$ were measured simultaneously. A Pt reference sample was measured to determine the Fermi level in XPS. The MPI end station is equipped with an MBE system connected directly to the measurement chamber. The growth conditions had to be slightly adjusted to account for the different growth environment.

III. RESULTS AND DISCUSSION

A. Growth study

To optimize the MBE growth conditions and to investigate the growth window, SmN films were grown on LAO (100) substrates in two series: a low nitrogen pressure series grown at $P_{N_2} = 1 \times 10^{-6}$ mbar and a high nitrogen pressure series grown at $P_{N_2} = 1 \times 10^{-5}$ mbar. The substrate temperature during growth was used as a variable parameter.

We begin this study with *in situ* RHEED measurements, which provide information about the crystalline growth of our films. Figure 1 displays the diffraction pattern of the substrate [Fig. 1(a)] as well as exemplary images of the low nitrogen pressure series [Figs. 1(b)–1(d)] and the high nitrogen pressure series [Figs. 1(e)–1(h)] taken immediately after deposition. We observe that the RHEED image corresponding to the film grown at room temperature ($T_{sub} = 25$ °C) and low nitrogen pressure [Fig. 1(b)] shows a diffraction pattern with

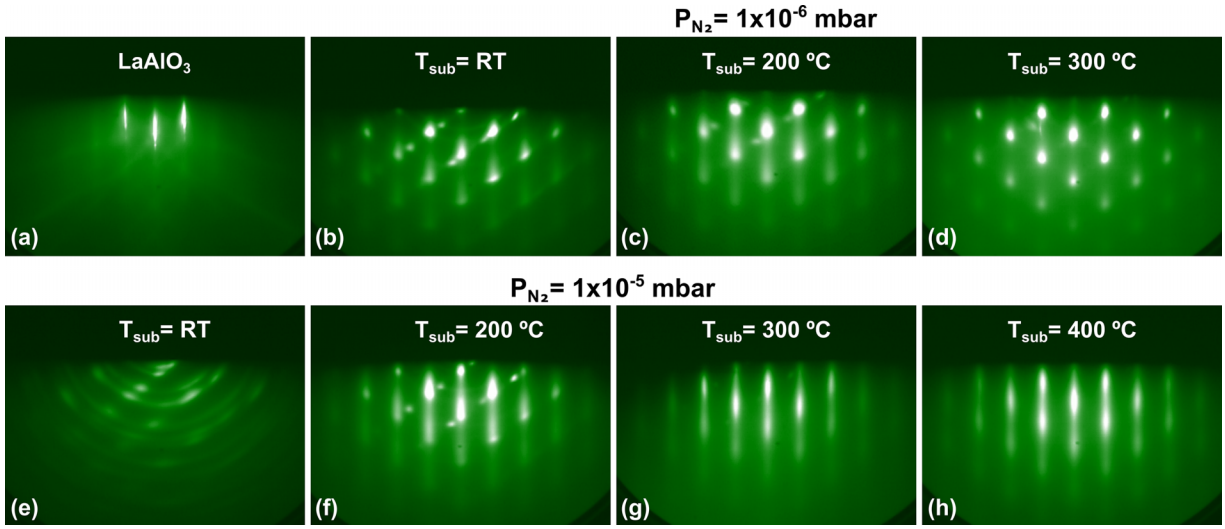

FIG. 1. *In situ* RHEED images of (a) the annealed $LaAlO_3$ (100) substrate before growth and of the SmN films grown at (b)–(d) $P_{N_2} = 1 \times 10^{-6}$ mbar and (e)–(h) $P_{N_2} = 1 \times 10^{-5}$ mbar and at the indicated substrate temperatures. The incident electron beam was aligned parallel to the [001] crystallographic direction of the $LaAlO_3$ substrate.

intense, elongated ordered spots and faint powder rings. This indicates predominantly three-dimensional epitaxial growth with some polycrystalline contribution [30]. In addition, there is a fainter second set of spots between the main spots, probably related to some texturing or structural reconstruction on the surface. At higher temperatures, the powder rings disappear [Figs. 1(c) and 1(d)], leaving only the transmission spots, which combine to form modulated diffraction streaks, indicating improved crystal growth. The second set of faint spots is still visible. RHEED images taken during the growth (not shown here) reveal an overall improvement in crystallinity over time.

If we compare these RHEED images with those obtained from films grown at high nitrogen pressure [Figs. 1(e)–1(h)], we observe that for the film grown at room temperature [Fig. 1(e)], the powder rings are more pronounced and the spots are less sharp than for its counterpart grown at lower pressure, indicating a lower degree of crystallinity. At $T_{sub} = 200\,^{\circ}C$ [Fig. 1(f)], the obtained RHEED pattern is similar to that grown at lower pressure, but with more streaky spots, implying that the films grow in multilevel stepped surfaces with a decreasing number of three-dimensional islands for the elevated temperature. The second set of faint spots mentioned previously is also visible. The RHEED pattern shows significant improvements for the higher substrate temperatures [Figs. 1(g) and 1(h)], for which we observe a mostly streaked pattern with some modulation, revealing a more two-dimensional growth character. The second set of faint spots is no longer present for these films. The crispness of the RHEED streaks indicates that high nitrogen pressure and a temperature of $300\,^{\circ}C$ [Fig. 1(g)] yield the best crystalline quality.

By utilizing the substrate as a reference for the spacing of the streaks [Fig. 1(a)] and assuming a 45° rotation of the SmN layer, we obtain an average lattice constant for all the grown films of about 5.0 ± 0.1 Å, which, within the accuracy of this technique, is in good agreement with the literature values of 5.0481 Å for this compound [13].

The composition of the films was monitored by XPS measurements. The wide scans (not shown here) displayed only the core levels related to samarium and nitrogen, demonstrating a high purity. Figure 2 shows the N 1*s* and Sm 4*d* core level spectra of the different films. We focus first on the Sm 4*d*

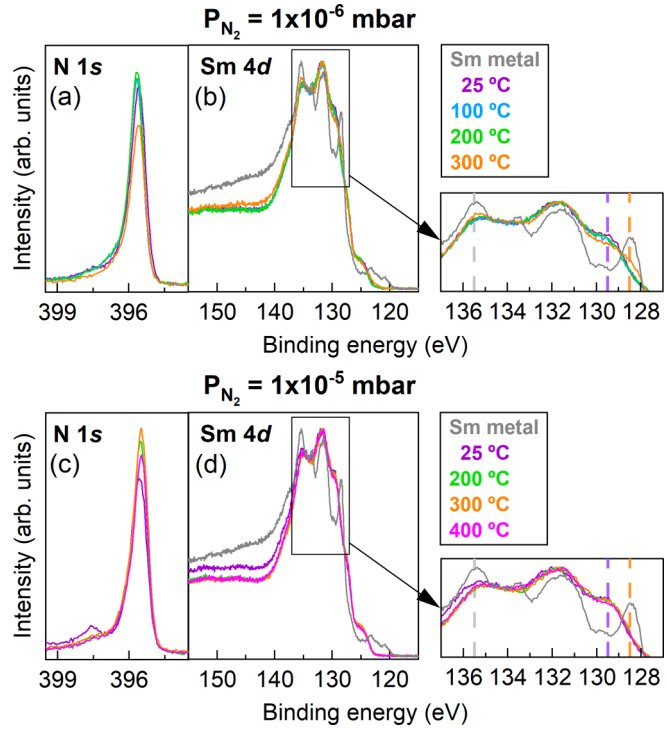

FIG. 2. N 1*s* and Sm 4*d* XPS spectra of the SmN films grown at (a) and (b) $P_{N_2} = 1 \times 10^{-6}$ mbar and (c) and (d) $P_{N_2} = 1 \times 10^{-5}$ mbar at the indicated temperatures. The N 1*s* spectra have been normalized to the integrated area of the corresponding Sm 4*d* spectra. The Sm 4*d* spectra have been normalized to their highest peak and are shown together with a Sm metal reference (gray). For clarity, close-ups of the Sm 4*d* spectra between 137 and 127 eV are shown.

spectra [Figs. 2(b) and 2(d)]. We observe that when compared to a Sm metal spectrum (gray line), the high-intensity features of the metal can be recognized in the nitride films, albeit with a significant broadening and smearing of the sharp features of the metal.

For the films grown at the low nitrogen pressure of 1×10^{-6} mbar [Fig. 2(b)], the Sm 4*d* spectra are similar across the series but exhibit some small differences. For the feature at 129.5 eV (purple dashed line in the close-up), the peak has the highest intensity for the film grown at room temperature (in purple), and its intensity decreases for films grown at higher temperatures, with the film grown at 300 °C (in orange) having the lowest intensity in this series. Additionally, we observe a small increase in the features characteristic of the Sm metal at 128.5 eV (orange dashed line) and at 135.5 eV (gray dashed line) for the film grown at 300 °C (in orange). These small changes are similar, albeit less noticeable, for the films grown at the high nitrogen pressure of 1×10^{-5} mbar [Fig. 2(d)], with only the film grown at the highest temperature (400 °C, in pink) exhibiting a lower intensity at the peak at 129.5 eV. Our results are similar to those found in the literature [27], with the features corresponding to the $4d^9 4f^5$ multiplets of Sm^{3+} [31]. The $4d^9 4f^6$ multiplets of Sm^{2+} [31], which are observed at about 123 and 121 eV for the Sm metal reference (Sm^{3+}/Sm^{2+} mixed valence surface [32,33]), are not present in our films.

The N 1*s* spectra [Figs. 2(a) and 2(c)] also show a trend. We observe that when normalized to the integrated area of the corresponding Sm 4*d* peak, the films grown at the intermediate temperatures of each series (100 and 200 °C at 1×10^{-6} mbar, 200 and 300 °C at 1×10^{-5} mbar) have the highest intensities of the main N 1*s* peak, indicating a higher nitrogen content for those films. Additionally, there is a noteworthy difference in the shape and intensity of N 1*s* for the film grown at room temperature and high nitrogen pressure [Fig. 2(c), in purple], which has an additional peak at ≈397.5 eV. This may be caused by some disorder in the film, which also explains the poor quality of the RHEED [Fig. 1(e)]. With the exception of the film grown at room temperature and high nitrogen pressure, the N 1*s* spectra show a sharp single peak with no clear additional features, confirming that the nitrogen reacts mainly in a single chemical environment and that there are no multiple nitrogen sites.

To obtain a more quantitative estimate of the stoichiometry of our films, we calculated the ratios of the integrated intensities of the N 1*s* and Sm 4*d* XPS core levels. A background was subtracted from all spectra as shown in the inset of Fig. 3. A Shirley (integral type) background was used for the Sm 4*d* core levels. For N 1*s*, a linear background was preferred. The integration range for each core level was kept constant for all samples. The ratios were calculated while taking into account the respective photoionization cross sections for the corresponding photon energy (0.1249 Mb for Sm 4*d* and 0.0240 Mb for N 1*s*) [34]. While the results derived from this method are not an absolute representation of the stoichiometry of the films due to potential differences between the surface and the bulk, systematic errors in the determination of the integrated intensities, analyzer efficiency, and photoionization cross sections, it is still a valuable method to understand the

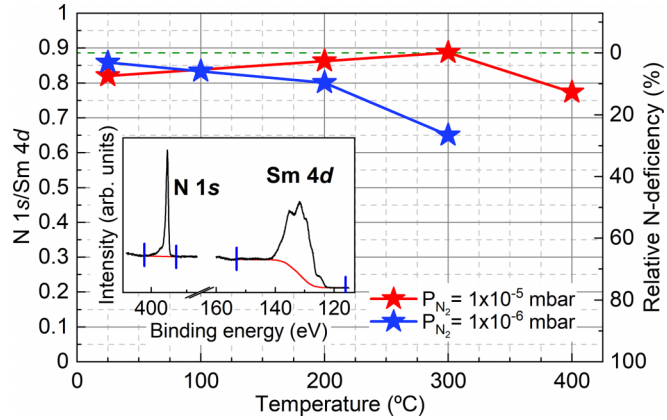

FIG. 3. N 1*s*/Sm 4*d* ratios calculated from the integrated intensities of the corresponding XPS spectra. The right axis shows the N deficiency relative to the highest ratio obtained in this study. As an example of the determination procedure, the inset displays the N 1*s* and Sm 4*d* core levels of a SmN film grown on $LaAlO_3$ (100) at 300 °C and $P_{N_2} = 1 \times 10^{-5}$ mbar (black), the subtracted background (red), and the integration range (blue).

effect of the substrate temperature and nitrogen pressure on the growth.

A summary of the results in Fig. 3 shows that the films grown at a nitrogen partial pressure of 1×10^{-6} mbar have an overall lower N 1*s*/Sm 4*d* ratio, with the exception of the film grown at room temperature, which has a slightly higher ratio than its high nitrogen pressure counterpart. Additionally, as mentioned previously for the normalized N 1*s* spectra of the low nitrogen pressure series [Fig. 2(a)], we observe that the ratio decreases for higher temperatures. A reduction in the nitrogen content of the films prepared at high growth temperatures was also found in other rare earth nitride studies and has generally been attributed to the formation of nitrogen vacancies [1,11,16,26,35]. For the films grown at $P_{N_2} = 1 \times 10^{-5}$ mbar, there is an increase of the N 1*s*/Sm 4*d* ratio with increasing temperature up to $T_{sub} = 300$ °C. For the film grown at high nitrogen pressure and 400 °C, we observed a slight increase of O 1*s* (not shown here). The origin of the oxygen contamination was investigated in detail for HoN thin films [26] and is likely caused by a migration of oxygen from the substrate to the film during the high-temperature growth, resulting in partial substitution of nitrogen by oxygen. We note that for all the films grown at lower temperatures, the level of oxygen immediately after growth is below the detection limit. Only after several hours of measurement do we observe that the O 1*s* core level increases slightly due to a slow oxidation of the surface even under ultrahigh-vacuum conditions.

The film grown at $T_{sub} = 300$ °C and $P_{N_2} = 1 \times 10^{-5}$ mbar has the highest N 1*s*/Sm 4*d* ratio that has been achieved in this study and is used as a reference to calculate the relative nitrogen deficiency, which we include as the right *y* scale in Fig. 3. The largest nitrogen deficiency of ≈27% is observed for the film grown at low nitrogen pressure and 300 °C.

With the insights gained from our growth study, we proceeded to prepare a thicker film (4 h deposition time) under the best growth conditions ($T_{sub} = 300$ °C, $P_{N_2} = 1 \times 10^{-5}$ mbar) with the intention of characterizing the crystalline structure in

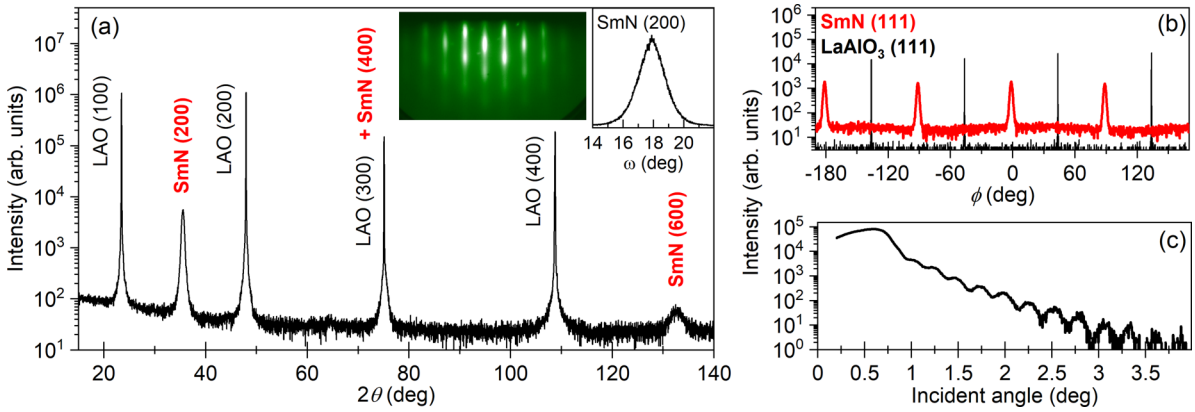

FIG. 4. Crystalline structure of a SmN thin film grown on $LaAlO_3$ (100) at the optimized conditions for 4 h. (a) XRD θ-2θ scan with the corresponding RHEED image and rocking curve. (b) In-plane ϕ scan. (c) XRR curve. The film was capped *in situ* with 10 nm of Cr for the XRD measurements.

more detail using *ex situ* XRD. To prevent degradation in air, the film was capped *in situ* with a 10 nm thick Cr layer.

The peaks in the XRD data [Fig. 4(a)] are consistent with those of the substrate or of the (2*n*00) family of SmN. The small feature at 65° can be attributed to the Cr of the capping layer. Other secondary phases are not observed. The XRD measurement yields a lattice constant of 5.05 Å, which is in agreement with the values published in the literature [13] and the RHEED results. The rocking curve around the SmN (200) reflection has a full width at half maximum of about 2°, comparable to that of other rare earth nitride films [28].

The in-plane ϕ scan [Fig. 4(b)] around the SmN (111) diffraction peak (in red) shows a fourfold set of peaks with a shift of 45° with respect to the pseudocubic lattice of the LAO substrate (in black), indicating that the SmN film is, indeed, growing at a 45° rotation with respect to the LAO substrate, as also indicated by RHEED.

From the period of the interference fringes in the x-ray reflectivity (XRR) measurement [Fig. 4(c)], we determine a film thickness of about 22 nm, indicating a SmN growth rate of approximately 0.93 Å/min.

B. Electronic structure of SmN

To investigate the influence of the nitrogen content on the Sm valence/4*f* configuration, *in situ* XPS and XAS measurements were performed at the TPS 45A beamline of the NSRRC, Taiwan. Figures 5–7 show the Sm 3*d* XPS spectra and the Sm $M_{4,5}$ edge and N *K* edge x-ray absorption spectra, respectively, for three SmN films with different nitrogen contents as determined from the Sm 4*d* and N 1*s* XPS core levels.

In Fig. 5, the XPS Sm 3*d* core level spectra of the SmN films are compared to Sm metal (black). The metal has a mixed valence surface and serves as a reference for the Sm^{3+} $3d^9 4f^5$ multiplet and Sm^{2+} $3d^9 4f^6$ multiplet energy positions. The features at around 1108 and 1081 eV have been assigned to the Sm^{3+} multiplets, the features at 1100 and 1073 eV have been assigned to the Sm^{2+} multiplets [32,36]. Thus, we can readily infer that the spectrum of the SmN film grown under optimized conditions (red curve) has clear features of the Sm^{3+} multiplets, while the Sm^{2+} multiplets are not present, indicating that the samarium ions in SmN have only the $4f^5$ configuration. Our Sm 3*d* spectrum is in agreement with measurements on Sm after nitridation reported in the literature [37]. The measurements on the nitrogen-deficient samples suggest that the $4f^5$ configuration of the samarium remains dominant even for a film with 19% less nitrogen (in blue). Only for the film with 30% less nitrogen (in green) are there small, but noticeable, changes near the energy positions of the Sm^{2+} multiplets, indicating the presence of some $4f^6$ configuration.

A similar trend was observed in the Sm $M_{4,5}$ absorption edges (Fig. 6). From a comparison of the spectrum of Sm_2O_3 of Kaindl *et al.* [38], which is a pure Sm^{3+} compound with only the $4f^5$ configuration, with our Sm metal reference, we can deduce that the feature at 1077 eV is related to the Sm^{2+} $4f^6$ configuration. This feature is not observed in the optimized SmN film or in the film with 19% less nitrogen. The spectra match rather closely the Sm_2O_3 data, thus further reinforcing the predominantly $4f^5$ configuration of the Sm in our films, even for the films with a significantly reduced

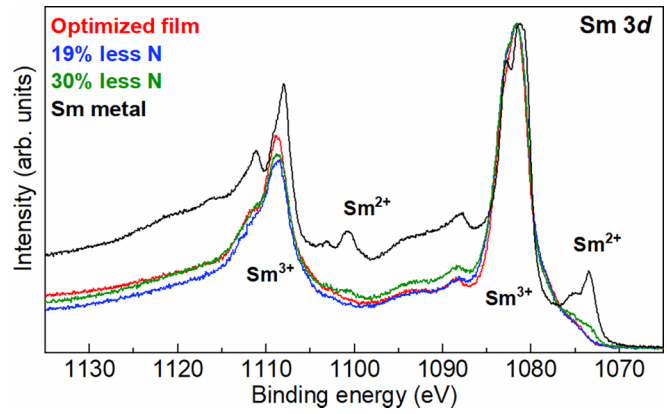

FIG. 5. Sm 3*d* XPS spectra of SmN films grown on $LaAlO_3$ (100) at 250 °C and $P_{N_2} = 1 \times 10^{-5}$ mbar (red, optimized conditions), at 200 °C and $P_{N_2} = 5 \times 10^{-7}$ mbar (blue, ≈19% less nitrogen), and at 300 °C and $P_{N_2} = 5 \times 10^{-7}$ mbar (green, ≈30% less nitrogen), together with a Sm metal reference spectrum (black). The spectra have been normalized to the highest intensity peak.

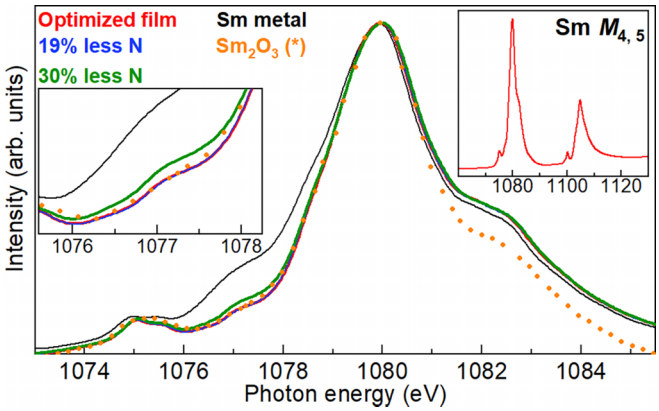

FIG. 6. XAS Sm $M_{4,5}$ edges of SmN films grown on $LaAlO_3$ (100) at 250 °C and $P_{N_2} = 1 \times 10^{-5}$ mbar (red, optimized conditions), at 200 °C and $P_{N_2} = 5 \times 10^{-7}$ mbar (blue, ≈19% less nitrogen), and at 300 °C and $P_{N_2} = 5 \times 10^{-7}$ mbar (green, ≈30% less nitrogen). A Sm metal reference spectrum (black) and a Sm_2O_3 reference [38] (orange dots) has been added. For clarity, a close-up of the Sm $M_{4,5}$ edges between 1075.5 and 1085.3 eV is displayed. The spectra have been normalized to the highest intensity peak.

nitrogen content. Moreover, the nearly perfect overlap of the Sm $M_{4,5}$ XAS spectra, which reflect the dipole-allowed $3d^{10}4f^n \longrightarrow 3d^9 4f^{n+1}$ multiplet transition of the rare earth ion, indicates that the Sm $4f$ states in SmN have a localized atomiclike behavior that is unaffected by considerable quantities of nitrogen vacancies. Only for the film with 30% less nitrogen is a small presence of the 1077 eV feature belonging to the Sm^{2+} $4f^6$ configuration detected, in agreement with the XPS data. The large number of nitrogen defects required for the signatures of the $4f^6$ configuration to occur could indicate that they are actually not related to the nitrogen defects per se, but rather to the formation of Sm metal clusters in the highly off-stoichiometric SmN films.

Our finding is surprising since nitrogen vacancies are known to act as electron donors in rare earth nitrides. As mentioned earlier, Sm has two stable valence states: Sm^{3+} ($[Xe]4f^5 5d^0$) and Sm^{2+} ($[Xe]4f^6 5d^0$), in contrast to many rare earth elements like Gd and Ho, which have a very stable 3+ valence. Thus, one might expect a different behavior upon electron doping. For SmN, the introduced electrons could lead to a reduction in the valence of the samarium ions. Holmes-Hewett proposed a model based on band structure calculations [39] in which roughly one of the three electrons per vacancy site is released to the six samarium ions which octahedrally coordinate the vacancy, resulting in an intermediate 2+/3+ valence for these ions, while the other two electrons are released into the valence band. Such a Sm^{2+} $4f^6$ contribution should be readily detectable by XPS and XAS even for only a few percent of vacancies. The absence of any signature of $4f^6$ even for a sample with 19% less nitrogen in our measurements thus raises an important question about where the extra electrons in the nitrogen-deficient compound are. One might speculate that the empty Sm $5d$ states play a role as a charge compensator, as has been observed for other compounds like SmB_6 [40,41]. Forming a $[Xe]4f^5 5d^1$ configuration near the vacancy, the Sm $5d$ states could act as a stabilizer for the $4f$ valence. The electrons in this Sm $5d$ state will eventually delocalize due to the large $5d$ bandwidth and will make the system metallic.

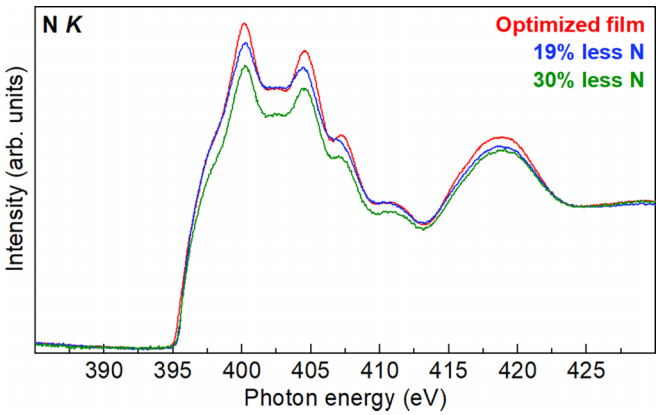

FIG. 7. XAS N K edges of SmN films grown on $LaAlO_3$ (100) at 250 °C and $P_{N_2} = 1 \times 10^{-5}$ mbar (red, optimized conditions), at 200 °C and $P_{N_2} = 5 \times 10^{-7}$ mbar (blue, ≈19% less nitrogen), and at 300 °C and $P_{N_2} = 5 \times 10^{-7}$ mbar (green, ≈30% less nitrogen). The spectra have been normalized to the edge jump at 430 eV.

We focus now on the N K absorption edges which probe the p-projected partial density of states of the conduction band (see Fig. 7). The spectrum of the optimized SmN film is in good agreement with measurements reported in the literature [14]. In contrast to the samarium edges, we observe a change in the nitrogen edges for samples with nitrogen deficiencies. While the overall shape of the N K edge absorption spectra does not change significantly, the intensity of the features is considerably reduced for the films with less nitrogen. Given that the two main peaks at about 400 and 405 eV have been associated with the rare earth $5d$ t_{2g} and e_g states [42], respectively, one might speculate that there are fewer holes in the $5d$ shell, supporting the idea that the extra electrons indeed occupy the empty Sm $5d$ shell rather than the $4f$ shell.

This leads us to the following picture: In stoichiometric SmN, the nitrogen takes three electrons from the samarium to form a Sm $4f^5$ configuration. In the presence of nitrogen vacancies, electrons are transferred back to the samarium, primarily occupying the $5d$ states; i.e., the Sm ions adopt a $4f^5 5d^1$ configuration. Only when a critical number of vacancies is exceeded and likely metal clusters are formed does the occupation of the $4f$ level, i.e., the formation of the $4f^6$ configuration, start to be energetically possible. This scenario may not be unrealistic if one considers, for example, the case of Sm metal. SmN and Sm metal have a similar close-packed Sm network with comparable Sm-Sm distances with a difference of only 1.3% [43]. In the metal, there are no nitrogen ions to absorb the electrons from the samarium. Still, the Sm ions have the $4f^5 5d^1$ configuration in the bulk, and only at the surface can Sm adopt the $4f^6$ configuration.

We now investigate the valence band (VB) of our SmN films in more detail for a better understanding of the electronic structure of SmN as calculations rely on the experimentally determined energy positions of the Sm $4f$ states [44]. Figure 8(a) shows the spectra of a single sample grown under optimized conditions taken at two different photon energies,

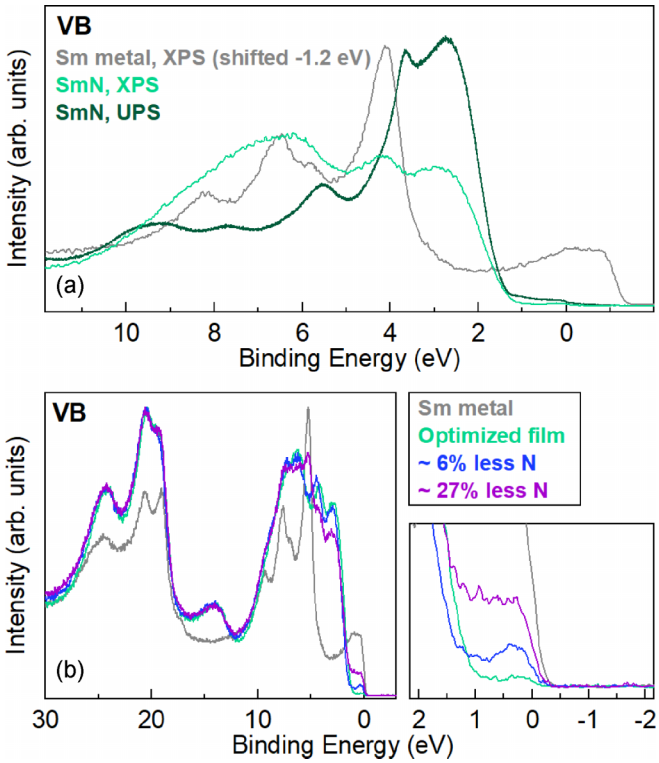

FIG. 8. (a) Valence band spectra measured with UPS (dark green) and XPS (teal) for a SmN film grown on $LaAlO_3$ (100) at 300 °C and $P_{N_2} = 1 \times 10^{-5}$ mbar. A reference Sm metal spectrum, shifted by −1.2 eV to match the Sm multiplets, is shown in gray. All spectra have been normalized to the integrated area between 11.85 and 1.15 eV. (b) XPS valence band spectra of SmN films grown on $LaAlO_3$ (100) at 300 °C and $P_{N_2} = 1 \times 10^{-5}$ mbar (teal), at 100 °C and $P_{N_2} = 1 \times 10^{-6}$ mbar (blue), and at 300 °C and $P_{N_2} = 1 \times 10^{-6}$ mbar (purple). A reference Sm metal spectrum is shown in gray. The SmN spectra have been normalized to the highest intensity peak. A close-up near the Fermi level is shown for clarity.

namely, 1486.6 eV (XPS) and 21.2 eV (UPS). The XPS spectrum of SmN (shown in teal) is compared to the spectrum of Sm metal (in gray). The Sm^{3+} $4f^5 \rightarrow 4f^4$ final states of both materials are expected to have a similar multiplet structure. The metal spectrum has been shifted by −1.2 eV to align the Sm multiplets. We observe that the Sm^{3+} multiplets of the metal [45] are also present in SmN, albeit with a significant level of broadening, which can also be seen in other samarium compounds [46]. However, the peak at ≈2.7 eV present in SmN has no counterpart in the metal spectrum. To identify the origin of this peak, we measure the valence band at a second photon energy to make use of the different photon energy dependences of the photoionization cross sections of the different elemental subshells. If we compare the photoionization cross sections for the Sm $4f$ and N $2p$ states (Table I), we notice that the Sm $4f$ states dominate for the XPS energy, while the N $2p$ states are emphasized for the UPS energy. Indeed, the valence band spectrum of the same sample measured by UPS [Fig. 8(a), in dark green] shows substantial differences compared to the XPS spectrum. For the lower photon energy we observe that, as expected from the cross sections in Table I, the features corresponding to

TABLE I. Photoionization cross sections of the Sm $4f^6$ and N $2p^3$ states for the photon energies used in this study [34].

	Cross section	
Photon energy	Sm $4f$ (Mb)	N $2p$ (Mb)
21.2 eV (UPS)	0.7216	9.688
1486.6 eV (XPS)	0.12×10^{-1}	0.72×10^{-4}

the Sm multiplets are highly suppressed and that the peak at 2.7 eV, which is present only in nitride, is enhanced, therefore indicating that it is related to the N $2p$ states. However, based on the reported cross-section values, the intensity of the N $2p$ states should be negligible compared to the samarium states for the XPS energy. That is in contrast to our observation, which shows a clear feature at the nitrogen position for the XPS measurement. This suggests that the peak at 2.7 eV has to be related to samarium which, in turn, indicates a considerable hybridization between the samarium and nitrogen states which was also predicted by calculations for this compound [47,48].

With the features of the SmN valence band successfully identified, we now compare the optimized film to the films with lower nitrogen contents. Figure 8(b) shows the XPS spectra for selected films grown under different conditions. These spectra were taken from the same films that are shown in Fig. 2. We observe that the 2.7 eV peak of the Sm $4f$ spectrum is at its highest intensity for the film grown under the optimized conditions (in teal) and this intensity decreases gradually for films with lower nitrogen contents, confirming the hybridization with the nitrogen states. Furthermore, the peak at ≈6 eV for the film with 27% less nitrogen (in purple) can be associated with Sm metal and thus indicates that the film might contain Sm metal clusters. This provides further evidence that the presence of the Sm^{2+} $4f^6$ multiplet features previously observed in the highly nitrogen-deficient sample (Figs. 5 and 6) is, indeed, related to metal clusters.

Last, if we focus on the area around the Fermi level [Fig. 8(b), close-up], we observe that for the film grown under optimized conditions (in teal) there is nearly no intensity at the Fermi level, confirming the semiconducting nature of stoichiometric SmN. The intensity at the Fermi level increases with decreasing nitrogen content. Comparing the results of all SmN samples measured, we find a clear correlation between the spectral weight at the Fermi level and the nitrogen content as obtained from the XPS core levels. Thus, considering the rather stable $4f^5$ configuration of Sm in SmN, the intensity at the Fermi level can serve as a qualitative indicator for the presence of nitrogen-vacancy-induced states of Sm $5d$ character. For the lower vacancy concentrations, defect states between 0 and 0.7 eV are formed which then merge into a broader band with a metallic Fermi cutoff, similar to what was observed in optical conductivity measurements on $SmN_{1-\delta}$ films [43].

IV. CONCLUSIONS

In summary, we successfully grew (100)-oriented epitaxial SmN films on $LaAlO_3$ (100) by means of MBE using molecular nitrogen and moderate growth conditions and showed that control over the nitrogen content can be achieved through

careful adjustments of the growth parameters. Combining XAS and XPS measurements, we were able to gain insights into the valence state of the samarium ions in SmN, showing its stable $4f^5$ configuration even for films with nitrogen vacancy concentrations of up to about 20%. Knowing that nitrogen vacancies act as electron donors, this suggests that the Sm $5d$ states may play a crucial role in the nitrogen-deficient compound, as the empty states can stabilize the Sm $4f$ valence by hosting the extra electrons ($4f^5 5d^1$ configuration). Only for the films with a very high nitrogen deficiency, which are expected to already contain metal clusters, did we observe features corresponding to Sm^{2+} $4f^6$ multiplets, which can likely be attributed to Sm ions located at the surface.

By taking advantage of the cross-section dependence of the Sm $4f$ and N $2p$ states for different photon energies, namely, by comparing XPS and UPS spectra from the same sample, we successfully identified the contributions to the valence band. Their photon energy dependence indicates that there is a significant hybridization of Sm with N. XPS measurements around the Fermi level confirmed the semiconducting behavior for stoichiometric SmN and showed an evolution from distinct defect states into a metalliclike band with a Fermi cutoff for films with an increasing number of nitrogen vacancies.

ACKNOWLEDGMENTS

The authors want to express their gratitude to C. Becker, K. Höfer, and T. Mende for their skillful technical assistance; to the department of C. Felser for the use of their thin film XRD instrument; to E. Lesne for the technical assistance; to P. Höhn for the purification of the samarium; and to S. Wirth for valuable discussions. For the experiments performed at TPS 45A (NSRRC, Taiwan), we thank H.-M. Tsai for technical assistance and the Max Planck-POSTECH-Hsinchu Center for Complex Phase Materials for support. A.M.-S. acknowledges the Material Science Ph.D. program of Universitat Autònoma de Barcelona and thanks M. I. Alonso from ICMAB-CSIC for her supervision.

[1] F. Natali, B. J. Ruck, N. O. V. Plank, H. J. Trodahl, S. Granville, C. Meyer, and W. R. L. Lambrecht, Rare-earth mononitrides, Prog. Mater. Sci. **58**, 1316 (2013).

[2] K. Senapati, M. G. Blamire, and Z. H. Barber, Spin-filter Josephson junctions, Nat. Mater. **10**, 849 (2011).

[3] H. Warring, B. J. Ruck, H. J. Trodahl, and F. Natali, Electric field and photo-excited control of the carrier concentration in GdN, Appl. Phys. Lett. **102**, 132409 (2013).

[4] D. Massarotti, A. Pal, G. Rotoli, L. Longobardi, M. G. Blamire, and F. Tafuri, Macroscopic quantum tunnelling in spin filter ferromagnetic Josephson junctions, Nat. Commun. **6**, 7376 (2015).

[5] R. Caruso, D. Massarotti, G. Campagnano, A. Pal, H. G. Ahmad, P. Lucignano, M. Eschrig, M. G. Blamire, and F. Tafuri, Tuning of magnetic activity in spin-filter Josephson junctions towards spin-triplet transport, Phys. Rev. Lett. **122**, 047002 (2019).

[6] J. D. Miller, F. H. Ullstad, H. J. Trodahl, B. J. Ruck, and F. Natali, Vertical transport and tunnelling in rare-earth nitride heterostructures, Nanotechnology **31**, 235202 (2020).

[7] G. Busch, P. Junod, F. Levy, A. Menth, and O. Vogt, Influence of crystal fields on the magnetic properties of the rare-earth nitrides, Phys. Lett. **14**, 264 (1965).

[8] D. P. Schumacher and W. E. Wallace, Magnetic characteristics of some lanthanide nitrides, Inorg. Chem. **5**, 1563 (1966).

[9] C. Meyer, B. J. Ruck, J. Zhong, S. Granville, A. R. H. Preston, G. V. M. Williams, and H. J. Trodahl, Near-zero-moment ferromagnetism in the semiconductor SmN, Phys. Rev. B **78**, 174406 (2008).

[10] E.-M. Anton, B. J. Ruck, C. Meyer, F. Natali, H. Warring, F. Wilhelm, A. Rogalev, V. N. Antonov, and H. J. Trodahl, Spin/orbit moment imbalance in the near-zero moment ferromagnetic semiconductor SmN, Phys. Rev. B **87**, 134414 (2013).

[11] J. F. McNulty, K. Temst, M. J. Van Bael, A. Vantomme, and E.-M. Anton, Epitaxial growth of (100)-oriented SmN directly on (100)Si substrates, Phys. Rev. Mater. **5**, 113404 (2021).

[12] H. Warring, H. J. Trodahl, N. O. V. Plank, F. Natali, S. Granville, and B. J. Ruck, Magnetic tunnel junctions incorporating a near-zero-moment ferromagnetic semiconductor, Phys. Rev. Appl. **6**, 044002 (2016).

[13] H. A. Eick, N. C. Baenziger, and L. Eyring, The preparation, crystal structure and some properties of SmN, EuN and YbN, J. Am. Chem. Soc. **78**, 5987 (1956).

[14] A. R. H. Preston, S. Granville, D. H. Housden, B. Ludbrook, B. J. Ruck, H. J. Trodahl, A. Bittar, G. V. M. Williams, J. E. Downes, A. DeMasi, Y. Zhang, K. E. Smith, and W. R. L. Lambrecht, Comparison between experiment and calculated band structures for DyN and SmN, Phys. Rev. B **76**, 245120 (2007).

[15] W. F. Holmes-Hewett, R. G. Buckley, B. J. Ruck, F. Natali, and H. J. Trodahl, Optical spectroscopy of SmN: Locating the $4f$ conduction band, Phys. Rev. B **99**, 205131 (2019).

[16] E.-M. Anton, S. Granville, A. Engel, S. V. Chong, M. Governale, U. Zülicke, A. G. Moghaddam, H. J. Trodahl, F. Natali, S. Vézian, and B. J. Ruck, Superconductivity in the ferromagnetic semiconductor samarium nitride, Phys. Rev. B **94**, 024106 (2016).

[17] J. W. Gerlach, J. Mennig, and B. Rauschenbach, Epitaxial gadolinium nitride thin films, Appl. Phys. Lett. **90**, 061919 (2007).

[18] B. M. Ludbrook, I. L. Farrell, M. Kuebel, B. J. Ruck, A. R. H. Preston, H. J. Trodahl, L. Ranno, R. J. Reeves, and S. M. Durbin, Growth and properties of epitaxial GdN, J. Appl. Phys. **106**, 063910 (2009).

[19] M. A. Scarpulla, C. S. Gallinat, S. Mack, J. S. Speck, and A. C. Gossard, GdN (111) heteroepitaxy on GaN (0001) by N_2 plasma and NH_3 molecular beam epitaxy, J. Cryst. Growth **311**, 1239 (2009).

[20] J. H. Richter, B. J. Ruck, M. Simpson, F. Natali, N. O. V. Plank, M. Azeem, H. J. Trodahl, A. R. H. Preston, B. Chen, J. McNulty, K. E. Smith, A. Tadich, B. Cowie, A. Svane, M. van Schilfgaarde, and W. R. L. Lambrecht, Electronic structure of EuN: Growth, spectroscopy, and theory, Phys. Rev. B **84**, 235120 (2011).

[21] B. J. Ruck, H. J. Trodahl, J. H. Richter, J. C. Cezar, F. Wilhelm, A. Rogalev, V. N. Antonov, B. D. Le, and C. Meyer, Magnetic state of EuN: X-ray magnetic circular dichroism at the Eu $M_{4,5}$ and $L_{2,3}$ absorption edges, Phys. Rev. B **83**, 174404 (2011).

[22] F. Natali, N. O. V. Plank, J. Galipaud, B. J. Ruck, H. J. Trodahl, F. Semond, S. Sorieul, and L. Hirsch, Epitaxial growth of GdN on silicon substrate using an AlN buffer layer, J. Cryst. Growth **312**, 3583 (2010).

[23] F. Natali, B. Ludbrook, J. Galipaud, N. Plank, S. Granville, A. Preston, B. L. Do, J. Richter, I. Farrell, R. Reeves, S. Durbin, J. Trodahl, and B. Ruck, Epitaxial growth and properties of GdN, EuN and SmN thin films, Phys. Status Solidi C **9**, 605 (2012).

[24] F. Natali, S. Vézian, S. Granville, B. Damilano, H. J. Trodahl, E.-M. Anton, H. Warring, F. Semond, Y. Cordier, S. V. Chong, and B. J. Ruck, Molecular beam epitaxy of ferromagnetic epitaxial GdN thin films, J. Cryst. Growth **404**, 146 (2014).

[25] J. R. Chan, S. Vézian, J. Trodahl, M. A. Khalfioui, B. Damilano, and F. Natali, Temperature-induced four-fold-on-six-fold symmetric heteroepitaxy, rocksalt SmN on hexagonal AlN, Cryst. Growth Des. **16**, 6454 (2016).

[26] V. M. Pereira, A. Meléndez-Sans, C. F. Chang, C.-Y. Kuo, C. T. Chen, L. H. Tjeng, and S. G. Altendorf, Epitaxial HoN thin films: An investigation of the structural, electronic, and magnetic properties, Phys. Rev. Mater. **7**, 124405 (2023).

[27] S. Vézian, B. Damilano, F. Natali, M. A. Khalfioui, and J. Massies, AlN interlayer to improve the epitaxial growth of SmN on GaN (0001), J. Cryst. Growth **450**, 22 (2016).

[28] E.-M. Anton, E. Trewick, W. F. Holmes-Hewett, J. R. Chan, J. F. McNulty, T. Butler, B. J. Ruck, and F. Natali, Growth of epitaxial (100)-oriented rare-earth nitrides on (100)$LaAlO_3$, Appl. Phys. Lett. **123**, 262401 (2023).

[29] F. Ullstad, G. Bioletti, J. R. Chan, A. Proust, C. Bodin, B. J. Ruck, J. Trodahl, and F. Natali, Breaking molecular nitrogen under mild conditions with an atomically clean lanthanide surface, ACS Omega **4**, 5950 (2019).

[30] S. Hasegawa, Reflection high-energy electron diffraction, in *Characterization of Materials* (Wiley, Hoboken, NJ, 2012), pp. 1–14.

[31] S. Suga, S. Imada, T. Jo, M. Taniguchi, A. Fujimori, S. J. Oh, A. Kakizaki, T. Ishii, T. Miyahara, T. Kasuya, A. Ochiai, and T. Suzuki, Photoemission, x-ray absorption, and inverse-photoemission studies of valence-fluctuating Sm_3Se_4, Phys. Rev. B **51**, 2061 (1995).

[32] G. K. Wertheim and G. Crecelius, Divalent surface state on metallic samarium, Phys. Rev. Lett. **40**, 813 (1978).

[33] O. Sakho, M. Sacchi, F. Sirotti, and G. Rossi, Valency changeover in Sm layers on Si(111)7 × 7 studied with soft-x-ray-absorption spectroscopy, Phys. Rev. B **47**, 3797 (1993).

[34] J. J. Yeh and I. Lindau, Atomic subshell photoionization cross sections and asymmetry parameters: $1 \leqslant Z \leqslant 103$, At. Data Nucl. Data Tables **32**, 1 (1985).

[35] W. F. Holmes-Hewett, R. G. Buckley, B. J. Ruck, F. Natali, and H. J. Trodahl, $4f$ conduction in the magnetic semiconductor NdN, Phys. Rev. B **100**, 195119 (2019).

[36] Y. Utsumi, D. Kasinathan, K.-T. Ko, S. Agrestini, M. W. Haverkort, S. Wirth, Y.-H. Wu, K.-D. Tsuei, D.-J. Kim, Z. Fisk, A. Tanaka, P. Thalmeier, and L. H. Tjeng, Bulk and surface electronic properties of SmB_6: A hard x-ray photoelectron spectroscopy study, Phys. Rev. B **96**, 155130 (2017).

[37] J. R. Chan, C. A. Casey-Stevens, M. Le Ster, A. Shaib, A. Tadich, B. C. C. Cowie, H. J. Trodahl, S. A. Brown, S. Granville, B. J. Ruck, A. L. Garden, and F. Natali, Epitaxial growth of gadolinium and samarium thin films and their subsequent facile nitridation at ambient temperatures, Appl. Surf. Sci. **632**, 157550 (2023).

[38] G. Kaindl, G. Kalkowski, W. D. Brewer, B. Perscheid, and F. Holtzberg, M-edge x-ray absorption spectroscopy of $4f$ instabilities in rare-earth systems (invited), J. Appl. Phys. **55**, 1910 (1984).

[39] W. F. Holmes-Hewett, Electronic structure of nitrogen-vacancy doped SmN: Intermediate valence and $4f$ transport in a ferromagnetic semiconductor, Phys. Rev. B **104**, 075124 (2021).

[40] M. Dzero, K. Sun, V. Galitski, and P. Coleman, Topological Kondo insulators, Phys. Rev. Lett. **104**, 106408 (2010).

[41] Z.-H. Zhu, A. Nicolaou, G. Levy, N. P. Butch, P. Syers, X. F. Wang, J. Paglione, G. A. Sawatzky, I. S. Elfimov, and A. Damascelli, Polarity-driven surface metallicity in SmB_6, Phys. Rev. Lett. **111**, 216402 (2013).

[42] A. R. H. Preston, B. J. Ruck, W. R. L. Lambrecht, L. F. J. Piper, J. E. Downes, K. E. Smith, and H. J. Trodahl, Electronic band structure information of GdN extracted from x-ray absorption and emission spectroscopy, Appl. Phys. Lett. **96**, 032101 (2010).

[43] W. F. Holmes-Hewett, K. Van Koughnet, J. D. Miller, E. X. M. Trewick, B. J. Ruck, H. J. Trodahl, and R. G. Buckley, Indications of a ferromagnetic quantum critical point in $SmN_{1-\delta}$, Sci. Rep. **13**, 19775 (2023).

[44] A. Galler and L. V. Pourovskii, Electronic structure of rare-earth mononitrides: Quasiatomic excitations and semiconducting bands, New J. Phys. **24**, 043039 (2022).

[45] G. K. Wertheim and M. Campagna, Is samarium metal in an intermediate valence state? Chem. Phys. Lett. **47**, 182 (1977).

[46] J. N. Chazalviel, M. Campagna, G. K. Wertheim, and P. H. Schmidt, Study of valence mixing in SmB_6 by x-ray photoelectron spectroscopy, Phys. Rev. B **14**, 4586 (1976).

[47] M. Topsakal and R. M. Wentzcovitch, Accurate projected augmented wave (PAW) datasets for rare-earth elements (RE = La-Lu), Comput. Mater. Sci. **95**, 263 (2014).

[48] C. Morari, F. Beiuşeanu, I. Di Marco, L. Peters, E. Burzo, S. Mican, and L. Chioncel, Magnetism and electronic structure calculation of SmN, J. Phys.: Condens. Matter **27**, 115503 (2015).